Progress In Electromagnetics Research, PIER 40, 315–333, 2003

SCATTERING BY A GYROTROPIC BIANISOTROPIC CYLINDER OF ARBITRARY CROSS SECTION: AN ANALYSIS USING GENERALIZED MULTIPOLE TECHNIQUE

M. Zhang, L. W. Li, T. S. Yeo, and M. S. Leong

Antenna and Scattering Laboratory
Department of Electrical and Computer Engineering
National University of Singapore
10 Kent Ridge Crescent, Singapore 119260

Abstract—The electromagnetic scattering by a homogeneous gyrotropic bianisotropic cylinder of arbitrary cross section is analyzed in this paper using the generalized multipole technique (GMT) where only the longitudinal fictitious electric and magnetic currents are involved. The general scattering solution is formulated and numerical results of near fields and bistatic radar cross sections are presented for four specific examples, namely, a chiral circular cylinder, a chiral square cylinder, a gyrotropic bianisotropic circular cylinder, and a gyrotropic bianisotropic "lens" cylinder. Results obtained using the GMT for the chiral and the gyrotropic bianisotropic circular cylinders are in excellent agreement with those obtained from the eigen-function expansion. Results of the GMT for the chiral square cylinder are in excellent agreement with those obtained from the method of moments (MoM) solution.

1. INTRODUCTION

A gyrotropic bianisotropic medium (GBM) is described by twelve scalar parameters in the following constitutive relations

$$\vec{D} = \tilde{\varepsilon} \cdot \vec{E} + \tilde{\xi} \cdot \vec{H}, \tag{1a}$$

$$\vec{B} = \tilde{\zeta} \cdot \vec{E} + \tilde{\mu} \cdot \vec{H}, \tag{1b}$$

where the constitutive dyadics $\tilde{\varepsilon}$, $\tilde{\mu}$, $\tilde{\xi}$, and $\tilde{\zeta}$ all take the form of

$$\tilde{g} = g_t \tilde{I}_t + g_c \hat{z} \times \tilde{I}_t + g_z \hat{z}\hat{z}, \tag{2}$$

or

$$\tilde{g} = \begin{bmatrix} g_t & -g_c & 0 \\ g_c & g_t & 0 \\ 0 & 0 & g_z \end{bmatrix}, \tag{3}$$

with $\tilde{I}_t$ being the transverse unit dyadic, and $\hat{z}$ being the unit vector in the z direction.

The electromagnetic scattering by an isotropic cylinder, i.e., with $\tilde{\varepsilon} = \varepsilon\tilde{I}$, $\tilde{\mu} = \mu\tilde{I}$, $\tilde{\xi} = 0$, and $\tilde{\zeta} = 0$, has been well-documented for a long time. In the case of $\tilde{\varepsilon} = \varepsilon\tilde{I}$, $\tilde{\mu} = \mu\tilde{I}$, and $\tilde{\xi} = -\tilde{\zeta} = j\xi_c\tilde{I}$, (3) is reduced to that of a chiral medium. The electromagnetic scattering by circular chiral cylinders and spheres have exact eigenfunction expansion solutions [1–4]. The scattering by a chiral cylinder of arbitrary cross section has also been analysed using the method of moments (MoM) [5, 6] and the generalized multipole technique (GMT) [7]. The scattering by a biisotropic cylinder, with $\tilde{\varepsilon} = \varepsilon\tilde{I}$, $\tilde{\mu} = \mu\tilde{I}$, $\tilde{\xi} = \xi\tilde{I}$, and $\tilde{\zeta} = \zeta\tilde{I}$, was studied in [8] using a contour integral technique. If $g_c = 0$ in (3), the material becomes uniaxial bianisotropic. The time-harmonic 2-D and 3-D closed form Green's dyadics for gyrotropic, bianisotropic, and anisotropic media were studied in [9]. The electromagnetic scattering by a uniaxial bianisotropic cylinder was presented in [10, 11]. In [10], the fictitious filament currents technique and the point matching method of generalized multipole technique have been applied. In [11], the vector wave function expansion method was used. Electromagnetic scattering by gyrotropic bianisotropic cylinders of some special shapes was analysed using equi-volumetric model [12] whereby a group of circular cylinders with different radii was used

to represent the original cylinder. As this method is an approximate one, the near field cannot be properly dealt with. If the cross section shape of the cylinder is complicated, a large number of these circular cylinders are needed and thus a lot of computation time is required. In [13], the Beltrami fields were applied to establish the volumetric integral equation for a general bianisotropic medium.

The early development and application of the generalized multipole technique (which was also called fictitious current method) were contributed by Hafner [14], Leviatan [15] and his colleagues [16, 17]. Recently, the generalized multipole technique was extended to deal with the scattering by underground scatterers [18], the scattering by conducting bodies of revolution [19], and the scattering by chiral and anisotropic cylinders [7, 20]. In [21, 22], the convergence and basis functions of the generalized multipole technique were discussed extensively.

In this paper, we present a generalized multipole technique solution for the problem of two-dimensional scattering of TE- and TM-polarized plane wave by an arbitrarily shaped homogeneous gyrotropic bianisotropic cylinder. Numerical results obtained for chiral circular and square cylinderes are compared to those computed using eigenfunction expansion and surface integral equations respectively. The scattering from circular and complex shaped gyrotropic bianisotropic cylinders are presented.

2. THEORETICAL FORMULATION

In this section, we describe in detail the problem formulation and its solution by the generalized multipole technique. Particular attention is given to the evaluation of Green's functions of the longitudinal currents in gyrotropic bianisotropic media and the Galerkin's technique in the generalized multipole technique.

2.1. Electromagnetic Fields in GBM Excited by Longitudinal Electric and Magnetic Currents

Consider a two-dimensional GBM cylinder located in free space and excited by a normally incident plane wave with the $e^{j\omega t}$ time dependence suppressed (Fig. 1).

The fields inside the cylinder and the operator ∇ can be decomposed into transverse components denoted by subscript t and a longitudinal component denoted by subscript z. From Maxwell's equations and the constitutive relations in (3), we have the fields in

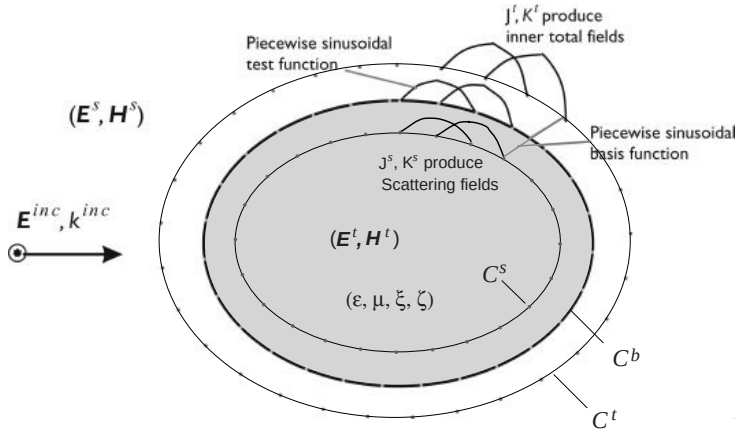

Figure 1. Geometry of a GBM cylinder and incident wave, configuration of basis functions of fictitious sources and testing functions.

the source free region as

$$\begin{bmatrix} -\zeta_t & -\mu_t & -\zeta_c & -\mu_c \\ \varepsilon_t & \xi_t & \varepsilon_c & \xi_c \\ \zeta_c & \mu_c & -\zeta_t & -\mu_t \\ -\varepsilon_c & -\xi_c & \varepsilon_t & \xi_t \end{bmatrix} \begin{bmatrix} \vec{E}_t \\ \vec{H}_t \\ \hat{z} \times \vec{E}_t \\ \hat{z} \times \vec{H}_t \end{bmatrix} = \frac{1}{j\omega} \begin{bmatrix} \nabla_t \times E_z \hat{z} \\ \nabla_t \times H_z \hat{z} \\ \nabla_t E_z \\ \nabla_t E_z \end{bmatrix}. \quad (4)$$

Inverting the coefficient matrix in the left-hand side of (4), we get the relation between the transverse and the longitudinal field components as

$$\begin{bmatrix} \vec{E}_t \\ \vec{H}_t \end{bmatrix} = \begin{bmatrix} V_{11} & V_{12} & V_{13} & V_{14} \\ V_{21} & V_{22} & V_{23} & V_{24} \end{bmatrix} \begin{bmatrix} \nabla_t \times E_z \hat{z} \\ \nabla_t \times H_z \hat{z} \\ \nabla_t E_z \\ \nabla_t E_z \end{bmatrix}, \quad (5)$$

where V_{ij} is the element of the inverse of the coefficient matrix in the left-hand side of (4). After the longitudinal components are solved for, the transverse field components can be obtained from (5) directly.

Now, consider the longitudinal components of fields when longitudinal electric current exists. From the Maxwell's equations and constitutive relations in (3), we have

$$\nabla_t^2 \begin{bmatrix} E_z \\ H_z \end{bmatrix} + [T] \begin{bmatrix} E_z \\ H_z \end{bmatrix} = [Q] J_z, \quad (6)$$

where

$$[T] = [A]^{-1}[B], \tag{7a}$$

$$[Q] = [A]^{-1}[C], \tag{7b}$$

$$[A] = \begin{bmatrix} j\omega(\zeta_c V_{13} + \mu_c V_{23}) - 1 & j\omega(\zeta_c V_{14} + \mu_c V_{24}) \\ j\omega(\varepsilon_c V_{13} + \xi_c V_{23}) & j\omega(\varepsilon_c V_{14} + \xi_c V_{24}) + 1 \end{bmatrix}, \tag{7c}$$

$$[B] = \omega^2 \begin{bmatrix} \mu_t\varepsilon_z - \zeta_t\zeta_z & \mu_t\xi_z - \zeta_t\mu_z \\ \xi_t\varepsilon_z - \varepsilon_t\zeta_z & \xi_t\xi_z - \varepsilon_t\mu_z \end{bmatrix}, \tag{7d}$$

$$[C] = -j\omega \begin{bmatrix} \mu_t \\ \xi_t \end{bmatrix}. \tag{7e}$$

We diagonalize the matrix as follows:

$$[a]^{-1}[T][a] = \begin{bmatrix} \gamma_+^2 & 0 \\ 0 & \gamma_-^2 \end{bmatrix}, \tag{8}$$

where $[a]$ is the eigenvector matrix of the matrix $[T]$ while γ_+ and γ_- are the eigenvalues of the matrix $[T]$. So the uncoupled fields

$$\begin{bmatrix} U_+ \\ U_- \end{bmatrix} = [a]^{-1} \begin{bmatrix} E_z \\ H_z \end{bmatrix} \tag{9}$$

satisfy the uncoupled wave equations

$$\nabla_t^2 \begin{bmatrix} U_+ \\ U_- \end{bmatrix} + \begin{bmatrix} \gamma_+^2 & 0 \\ 0 & \gamma_-^2 \end{bmatrix} \begin{bmatrix} U_+ \\ U_- \end{bmatrix} = \begin{bmatrix} C_+ \\ C_- \end{bmatrix} J_z, \tag{10}$$

where $\begin{bmatrix} C_+ \\ C_- \end{bmatrix} = [a]^{-1}[C]$. It is clear that the Green's functions of $U_\pm$ take the form of

$$G_\pm(\gamma_\pm|\vec{\rho} - \vec{\rho}'|) = -\frac{j}{4} H_0^{(2)}(\gamma_\pm|\vec{\rho} - \vec{\rho}'|), \tag{11}$$

where $H_0^{(2)}(\cdot)$ is the Hankel function of the zeroth order and the second kind, $\vec{\rho}$ and $\vec{\rho}'$ are position vectors of field point and source point, respectively. Therefore, the E_z and the H_z excited by $J_z(\vec{\rho}')$ which is distributed in the area of S can be written as

$$\begin{bmatrix} E_z(\vec{\rho}) \\ H_z(\vec{\rho}) \end{bmatrix} = -\frac{j}{4} \int_S [a] \begin{bmatrix} C_+ H_0^{(2)}(\gamma_+|\vec{\rho} - \vec{\rho}'|) \\ C_- H_0^{(2)}(\gamma_-|\vec{\rho} - \vec{\rho}'|) \end{bmatrix} J_z(\vec{\rho}') d\vec{\rho}'. \tag{12}$$

The transverse components of fields in the cylindrical coordinates can be obtained from (5), given by

$$\begin{bmatrix} E_\rho \\ E_\phi \\ H_\rho \\ H_\phi \end{bmatrix} = \begin{bmatrix} V_{11} & V_{12} & V_{13} & V_{14} \\ V_{13} & V_{14} & -V_{11} & -V_{12} \\ V_{21} & V_{22} & V_{23} & V_{24} \\ V_{23} & V_{24} & -V_{21} & -V_{22} \end{bmatrix} \begin{bmatrix} \frac{1}{\rho}\frac{\partial E_z}{\partial \phi} \\ \frac{1}{\rho}\frac{\partial H_z}{\partial \phi} \\ \frac{\partial E_z}{\partial \rho} \\ \frac{\partial H_z}{\partial \rho} \end{bmatrix}, \tag{13}$$

and

$$\begin{bmatrix} \frac{1}{\rho}\frac{\partial E_z}{\partial \phi} \\ \frac{1}{\rho}\frac{\partial H_z}{\partial \phi} \end{bmatrix} = -\frac{j}{4} \cdot \frac{\rho' \sin(\phi - \phi')}{|\vec{\rho} - \vec{\rho}'|}[a] \begin{bmatrix} C_+\gamma_+ H_0^{(2)'}(\gamma_+|\vec{\rho} - \vec{\rho}'|) \\ C_-\gamma_- H_0^{(2)'}(\gamma_-|\vec{\rho} - \vec{\rho}'|) \end{bmatrix}, \tag{14a}$$

$$\begin{bmatrix} \frac{\partial E_z}{\partial \rho} \\ \frac{\partial H_z}{\partial \rho} \end{bmatrix} = -\frac{j}{4} \cdot \frac{\rho - \rho' \cos(\phi - \phi')}{|\vec{\rho} - \vec{\rho}'|}[a] \begin{bmatrix} C_+\gamma_+ H_0^{(2)'}(\gamma_+|\vec{\rho} - \vec{\rho}'|) \\ C_-\gamma_- H_0^{(2)'}(\gamma_-|\vec{\rho} - \vec{\rho}'|) \end{bmatrix}, \tag{14b}$$

By means of a duality transformation, i.e., $\vec{E} \leftrightarrow \vec{H}$, $J_z \leftrightarrow -K_z$, $\tilde{\varepsilon} \leftrightarrow -\tilde{\mu}$, and $\tilde{\xi} \leftrightarrow -\tilde{\zeta}$, the electromagnetic fields due to a longitudinal magnetic current density source K_z can thus be obtained.

2.2. GMT Solution

In the generalized multipole technique model, the unknown fields (external scattered fields and internal transmitted fields) are usually expanded in terms of the eigenfunctions with undetermined magnitudes. The fields satisfy exactly the wave equations with respect to different regions and different coordinate origins. The boundary conditions are then enforced at numerous collocation points to determine the expansion coefficients. For convenience of computation, only the fields which are excited by the electric and magnetic axial filament currents are considered [7, 10]. It has been pointed out [22] that, filament (impulse) currents representation of the fictitious sources would lead to much larger error in the point-matching of the boundary conditions and consequently difficulty in the convergence of the final results. As such, the piecewise sinusoidal

basis functions are used in this paper to represent the fictitious sources and as testing functions. We further model the fictitious sources as longitudinal electric and magnetic currents since the field expressions for longitudinal components have very simple forms [7, 10].

From Fig. 1, the fictitious electric and magnetic currents exciting the total electromagnetic fields inside the scatterer can be expanded by the PWS basis functions, i.e.,

$$J_z^t(\vec{\rho}'^t) = \sum_{n=1}^{N} J_n^t f^t(\vec{\rho}'^t), \tag{15a}$$

$$K_z^t(\vec{\rho}'^t) = \sum_{n=1}^{N} K_n^t f^t(\vec{\rho}'^t), \tag{15b}$$

where $\vec{\rho}'^t \in C^t$. The fictitious electric and magnetic currents exciting the scattered electromagnetic fields outside the scatterer can be expanded by the PWS basis functions in a similar form

$$J_z^s(\vec{\rho}'^s) = \sum_{n=1}^{N} J_n^s f^s(\vec{\rho}'^s), \tag{16a}$$

$$K_z^s(\vec{\rho}'^s) = \sum_{n=1}^{N} K_n^s f^s(\vec{\rho}'^s), \tag{16b}$$

where $\vec{\rho}'^s \in C^s$, and the superscripts t and s refer to the internal fields and scattered (external) fields, respectively.

By enforcing the boundary conditions with respect to the subdomain testing functions along the surface of the cylinder C^b, we obtain the following operator equations after expanding the electric and magnetic currents with PWS basis functions:

$$\begin{aligned}\left\langle E_z^i, g(\vec{\rho}_m)\right\rangle = \sum_{n=1}^{N} \Big\{ & J_n^t \left\langle L_{E_z J_z^t}\left[f^t(\vec{\rho}'^t_n)\right], g(\vec{\rho}_m)\right\rangle \\ & + K_n^t \left\langle L_{E_z K_z^t}\left[f^t(\vec{\rho}'^t_n)\right], g(\vec{\rho}_m)\right\rangle \\ & - J_n^s \left\langle L_{E_z J_z^s}\left[f^s(\vec{\rho}'^s_n)\right], g(\vec{\rho}_m)\right\rangle \Big\},\end{aligned} \tag{17a}$$

$$\begin{aligned}\left\langle E_t^i, g(\vec{\rho}_m)\right\rangle = \sum_{n=1}^{N} \Big\{ & J_n^t \left\langle L_{E_z J_z^t}\left[f^t(\vec{\rho}'^t_n)\right], g(\vec{\rho}_m)\right\rangle \\ & + K_n^t \left\langle L_{E_z K_z^t}\left[f^t(\vec{\rho}'^t_n)\right], g(\vec{\rho}_m)\right\rangle \\ & - K_n^s \left\langle L_{E_z K_z^s}\left[f^s(\vec{\rho}'^s_n)\right], g(\vec{\rho}_m)\right\rangle \Big\},\end{aligned} \tag{17b}$$

$$\left\langle H_z^i, g(\vec{\rho}_m)\right\rangle = \sum_{n=1}^{N}\Big\{J_n^t\left\langle L_{H_zJ_z^t}\left[f^t(\vec{\rho}\,'^t{}_n)\right], g(\vec{\rho}_m)\right\rangle + K_n^t\left\langle L_{H_zK_z^t}\left[f^t(\vec{\rho}\,'^t{}_n)\right], g(\vec{\rho}_m)\right\rangle - K_n^s\left\langle L_{H_zK_z^s}\left[f^s(\vec{\rho}\,'^s{}_n)\right], g(\vec{\rho}_m)\right\rangle\Big\}, \tag{17c}$$

$$\left\langle H_t^i, g(\vec{\rho}_m)\right\rangle = \sum_{n=1}^{N}\Big\{J_n^t\left\langle L_{H_tJ_z^t}\left[f^t(\vec{\rho}\,'^t{}_n)\right], g(\vec{\rho}_m)\right\rangle + K_n^t\left\langle L_{H_tK_z^t}\left[f^t(\vec{\rho}\,'^t{}_n)\right], g(\vec{\rho}_m)\right\rangle - J_n^s\left\langle L_{H_tJ_z^s}\left[f^s(\vec{\rho}\,'^s{}_n)\right], g(\vec{\rho}_m)\right\rangle\Big\}, \tag{17d}$$

where $m = 1, 2, \ldots, N$, $\langle A, B\rangle$, denotes the inner product of A and B, and $g(\vec{\rho}_m)$ is a testing function, we chose the PWS function here. It is similar to the Galerkin's technique in the MoM. The subscript t denotes transverse tangential component, and superscript i denotes incident wave. $L_{E_zJ_z^t}$, $L_{E_tJ_z^t}$, $L_{H_zJ_z^t}$ and $L_{H_tJ_z^t}$ are the operators which are used to calculate E_z, E_t, H_z and H_t from J_z in GBM respectively. $L_{E_zK_z^t}$, $L_{E_tK_z^t}$, $L_{H_zK_z^t}$ and $L_{H_tK_z^t}$ are the operators which are used to calculate E_z, E_t, H_z and H_t from K_z in GBM respectively. $L_{E_zJ_z^s}$, and $L_{H_tJ_z^s}$ are the operators used to calculate E_z and E_t from J_z in free space respectively. $L_{H_zK_z^s}$ and $L_{E_tK_z^s}$ are the operators which are used to calculate H_z and E_t from K_z in free space respectively.

Subsequently, the $4N$ linear equations given in (17a) to (17d) can be solved for the $4N$ unknowns J_n^t, K_n^t, J_n^s and K_n^s directly using Gaussian elimination or iteration methods. After the complex magnitude coefficients of the fictitious currents are obtained, the external scattered fields and internal total fields can be calculated from these fictitious currents.

3. NUMERICAL RESULTS AND DISCUSSIONS

We present in this Section, the convergence of GMT, the bistatic RCS and the near-zone electric and magnetic fields of various chiral and GBM cylinders. The results were computed at 300 MHz (free space wavelength λ_0 is 1 meter).

3.1. Circular Chiral Cylinder

The first example is the scattering of a TM-polarized incident plane wave by a circular chiral cylinder. The radius of the cylinder is $0.1\,\lambda_0$. The cylinder is lossless and has the parameters $\varepsilon_t = \varepsilon_z = 1.642\varepsilon_0$, $\varepsilon_c =$

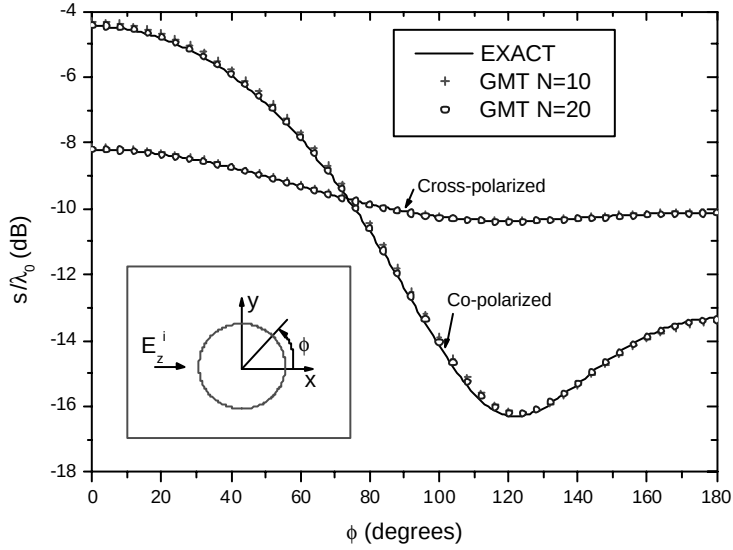

Figure 2. The co-polarized and cross-polarized bistatic RCS of a circular chiral cylinder illuminated by a TM-polarized incident plane wave.

0, $\mu_t = \mu_z = 4.0\mu_0$, $\mu_c = 0$, $\xi_t = \xi_z = j0.754\sqrt{\varepsilon_0\mu_0}$, $\xi_c = 0$, $\zeta_t = \zeta_z = -\xi_t$, and $\zeta_c = 0$. The bistatic radar cross sections obtained by using the eigenfunction expansion method and the GMT are compared in Fig. 2. We can see that when $N \geq 10$, the results of co-polarized and cross-polarized RCS are agreed excellent with those of the exact solution. When $N = 10$, the size of the moment matrix is 40*40 in the GMT. The convergence of the GMT is much faster than the volume integral equation in [5] and the surface integral equation in [6]. In [5], 63 cells and a moment matrix with the size of 378*378 were used. In [6], 44 segments and a moment matrix with the size of 176*176 were used. There are two reasons of the fast convergence of the GMT. The first is that the GMT is a method like the surface integral equation method, which is superior to the volume integral equation methods for solving a homogenous object problem. The second is that the PWS are used as the basis functions as well as the test functions in the GMT. The PWS basis function associated with the Galerkin's technique has a faster convergence than the pulse basis function and point matching approach, which was used in [6].

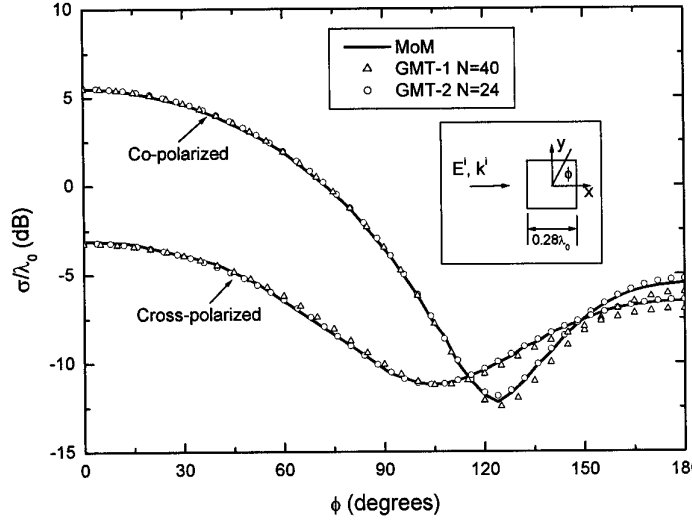

Figure 3. The co-polarized and cross-polarized bistatic RCS of a square chiral cylinder in the TM-polarized incident case.

3.2. Square Chiral Cylinder

The second example is the scattering of a TM-polarized incident plane wave by a square chiral cylinder. The bistatic RCSs obtained using the current GMT, denoted by GMT-2, are compared in Fig. 3 with those obtained using MoM [6] and the original GMT, where the impulsive basis function and the point match are used, denoted by GMT-1. The dielectric and geometrical parameters used are the same as those given in [6]: $\varepsilon_t = \varepsilon_z = 3.071\varepsilon_0$, $\varepsilon_c = 0$, $\mu_t = \mu_z = 2.0\mu_0$, $\mu_c = 0$, $\xi_t = \xi_z = j0.3767\sqrt{\varepsilon_0\mu_0}$, $\xi_c = 0$, $\zeta_t = \zeta_z = -\xi_t$, and $\zeta_c = 0$. To efficiently match the boundary conditions, the boundary of the cylinder is divided into *24* equal segments (*6* segments each side), and the size of the moment matrix used is the size of 96×96. The magnitude of the internal electric field E_y along the $y = 0$ line was also computed and is shown in Fig. 4. It can be seen that these results are in excellent agreement, and the covergence of the GMT when using pws as basis functions and test functions is better than that of using impulsive basis functions and point match.

3.3. Circular GBM Cylinder

The third example is the scattering of TM- and TE-polarized incident plane waves by a circular GBM cylinder. The radius of the cylinder is

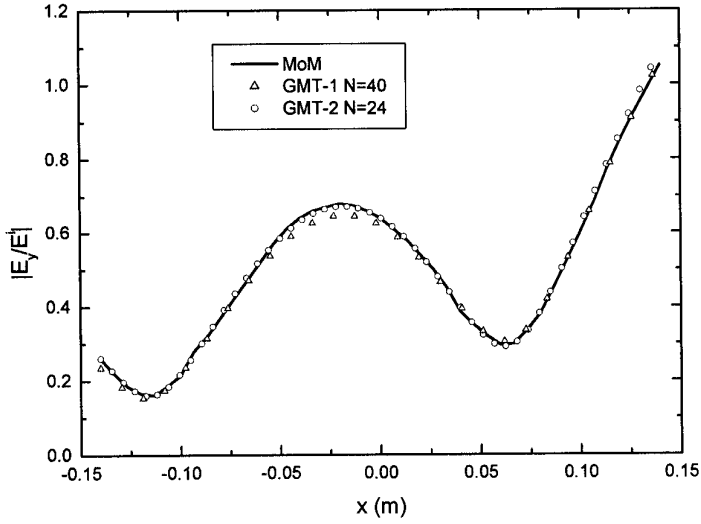

Figure 4. Internal E_y along $y = 0$ line.

taken to be 1 λ_0. The cylinder is lossy in nature and its parameters are taken to be: $\varepsilon_t = (2 - j0.5)\varepsilon_0$, $\varepsilon_z = (3 - j1.5)\varepsilon_0$, $\varepsilon_c = (0.5 - j0.2)\varepsilon_0$, $\mu_t = (4 - j0.05)\mu_0$, $\mu_z = (2 - j0.1)\mu_0$, $\mu_c = (0.3 - j0.1)\mu_0$, $\xi_t = (1 - j0.1)\sqrt{\varepsilon_0\mu_0}$, $\xi_z = (0.8 - j0.2)\sqrt{\varepsilon_0\mu_0}$, $\xi_c = (0.5 - j0.1)\sqrt{\varepsilon_0\mu_0}$, $\zeta_t = (-0.1 - j0.9)\sqrt{\varepsilon_0\mu_0}$, $\zeta_z = (-0.2 - j0.8)\sqrt{\varepsilon_0\mu_0}$, $\zeta_c = (0.3 - j0.2)\sqrt{\varepsilon_0\mu_0}$. Fig. 5(a), (b) show the convergence of the GMT for computing co- and cross-polarized bistatic RCS for a GBM circular cylinder illuminated by a TM incident wave. It can be seen that the RCS obtained by the GMT are agreed with the exact solutions very well when $N \geq 60$. The near-zone electric and magnetic fields along x axis are shown in Fig. 6 and Fig. 7, respectively. Figure 8 shows the TE bistatic RCS. The near-zone electric and magnetic fields along x axis are shown in Fig. 9 and Fig. 10, respectively.

It is seen from these results that, unlike the case for scattering by a uniaxial bianisotropic circular cylinder, the co- and cross-polarized RCS of a GBM circular cylinder is not symmetrical with respect to the scattering angle ϕ, due to the existence of nonzero non-diagonal elements in the constitution relation [23], although the problem has geometric symmetry. Also, the cross-polarized radar cross sections for the TM and TE cases are not identical, unlike the chiral medium case [4], due to the non-reciprocal property of the constitutive parameters. Along the $-x$ direction, the E_z and the H_y components for TM case and the H_z and the E_y components for TE case, dominate the electric and magnetic fields respectively. The co-polarized components

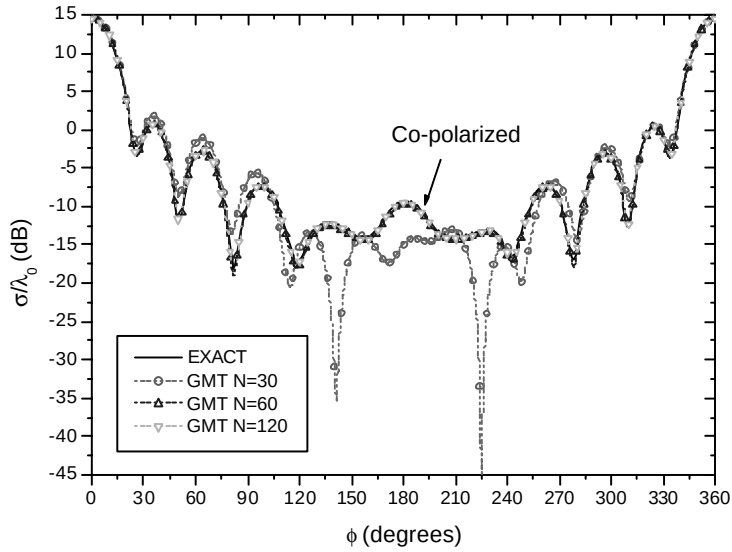

(a) Co-polarized bistatic RCS

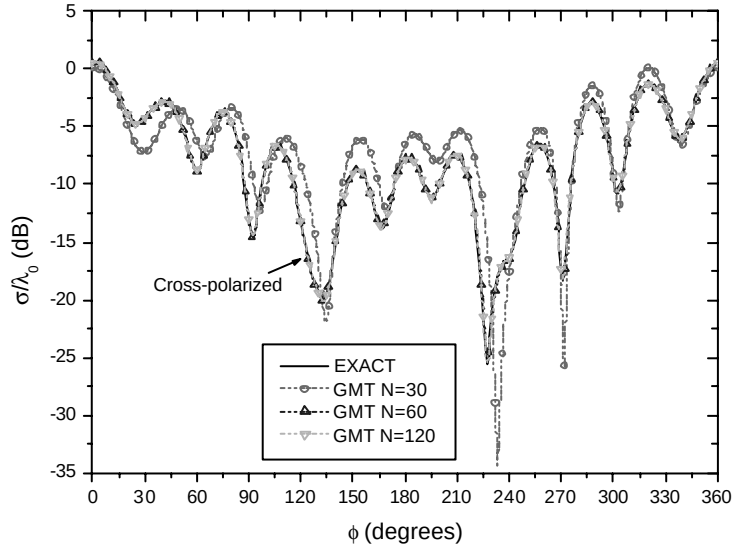

(b) Cross-polarized bistatic RCS

Figure 5. Bistatic RCS of a GBM circular cylinder in the case of TM-polarized incident wave.

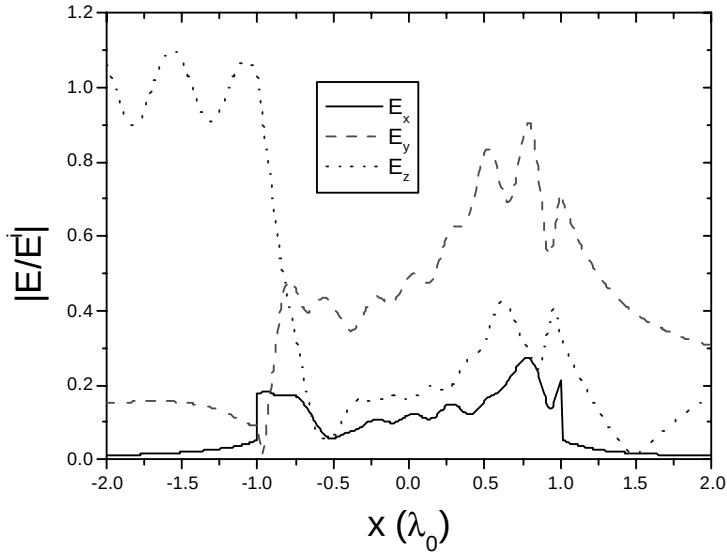

Figure 6. Near-zone electric fields of a GBM circular cylinder (TM case).

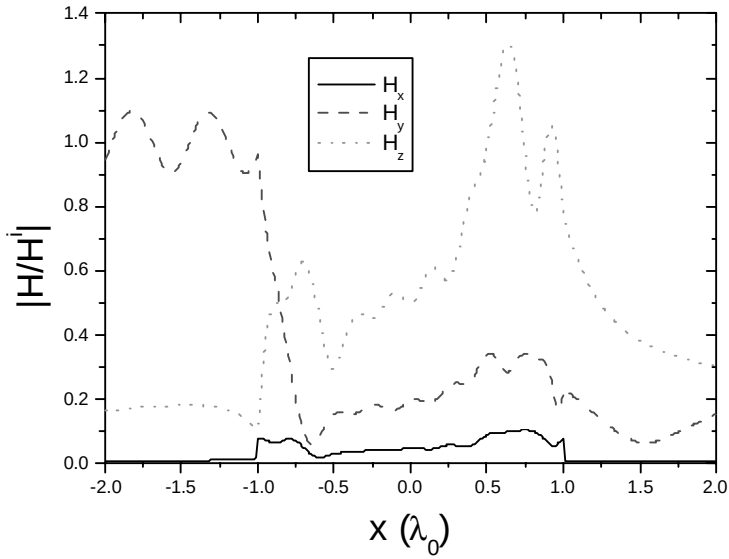

Figure 7. Near-zone magnetic fields of a GBM circular cylinder (TM case).

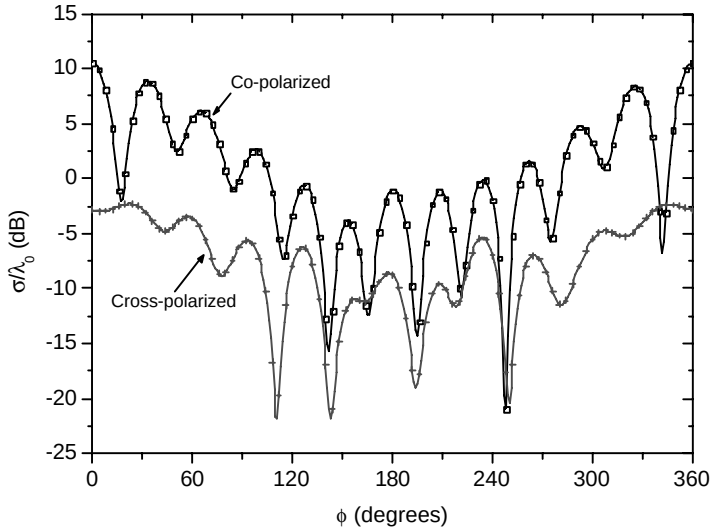

Figure 8. RCS of a GBM circular cylinder in the case of TE-polarized incident wave.

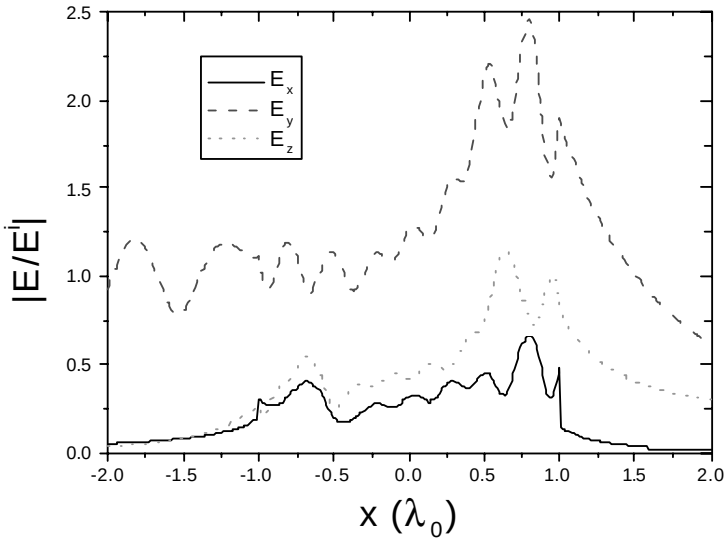

Figure 9. Near-zone electric fields of a GBM circular cylinder (TE case).

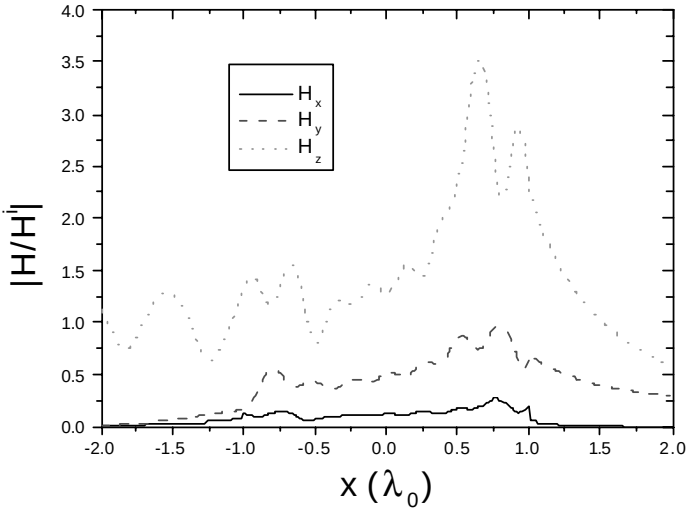

Figure 10. Near-zone magnetic fields of a GBM circular cylinder (TE case).

penetrate into, and peaked within, the cylinder. However, once outside, they decay rapidly. On the other hand, the cross-polarized components, the E_y and the H_z components for TM-case and the H_y and the E_z components for TE-case, decay at a much slower rate. In all cases, the E_x and the H_x components do not contribute significantly to the total electromagnetic fields both inside and outside of the cylinder. It is also observed that after the incident wave enters into the cylinder, the contribution of all the components due to the incident wave is increased, especially around the second interface.

3.4. GBM Lens Cylinder

Finally, the scattering of a TM-polarized incident plane wave by a $5\,\lambda_0$-radius GBM "lens" cylinder (Fig. 11 insert) with $\alpha = 45^\circ$ is investigated. Figure 11 presents the bistatic radar cross sections of this GBM "lens" cylinder while Figs. 12 and 13 provide the near-zone electric and magnetic fields along the $y = 0$ line respectively. Although the method itself can handle lossy material, the cylinder is assumed to be lossless in this computation. The following parameters are used: $\varepsilon_t = 2\varepsilon_0,\ \varepsilon_z = 3\varepsilon_0,\ \varepsilon_c = j0.5\varepsilon_0,\ \mu_t = 4\mu_0,\ \mu_z = 2\mu_0,\ \mu_c = j0.3\mu_0,\ \xi_t = j0.5\sqrt{\varepsilon_0\mu_0},\ \xi_z = j0.6\sqrt{\varepsilon_0\mu_0},\ \xi_c = 0.2\sqrt{\varepsilon_0\mu_0},\ \zeta_t = -j0.5\sqrt{\varepsilon_0\mu_0},\ \zeta_z = -j0.7\sqrt{\varepsilon_0\mu_0},\ \zeta_c = -0.2\sqrt{\varepsilon_0\mu_0}$.

It can be seen from Figs. 11 to 13 that the transverse back-

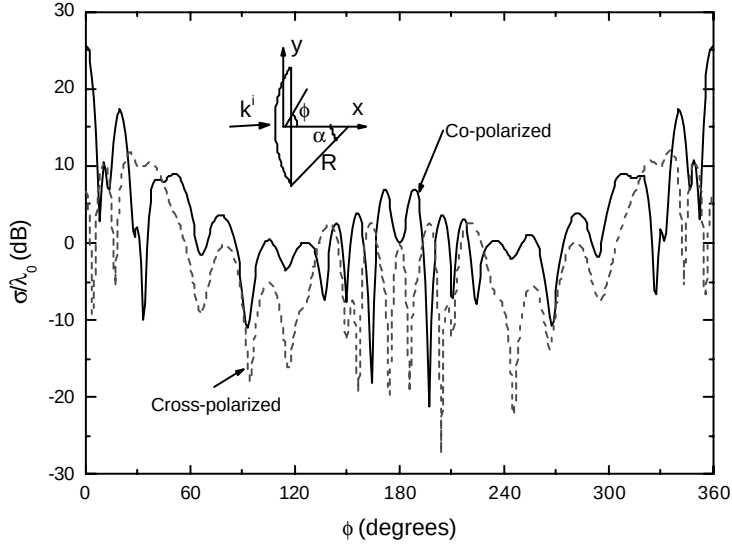

Figure 11. RCS of a GBM lens cylinder in the TM-polarization case.

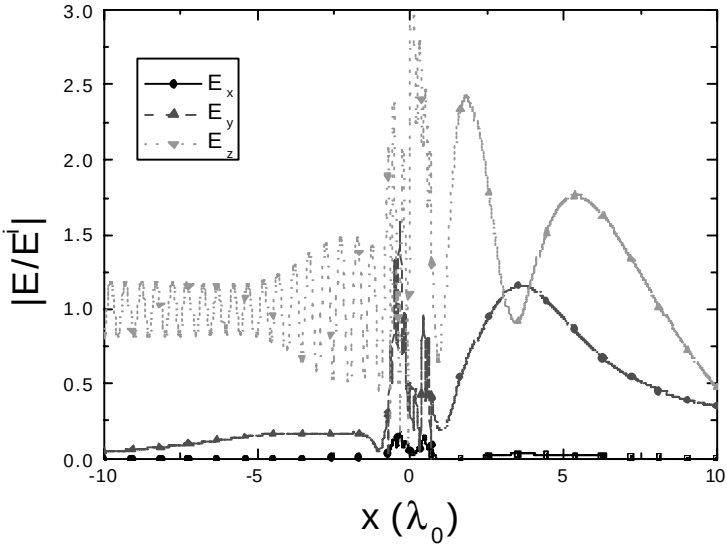

Figure 12. Near electric fields along $y = 0$ line.

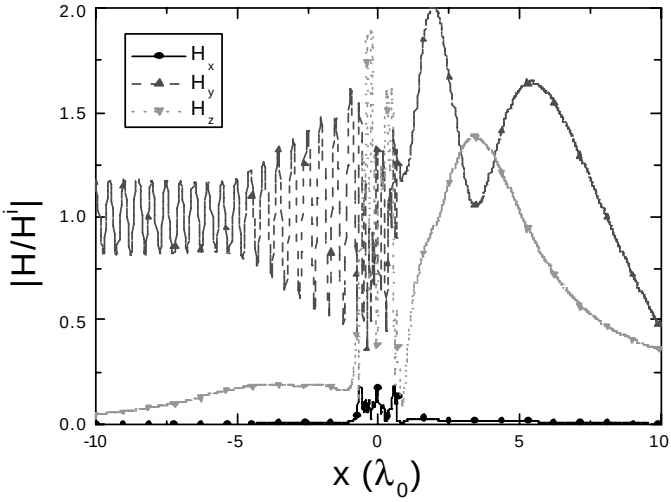

Figure 13. Near magnetic fields along $y = 0$ line.

scattered field components take on a standing wave behaviour due to the strong reflection from the planar and near-planar interfaces. Within and close to the scatterer, the fields oscillate wildly due to the strong interaction. This phenomenon is true for all the six components of the electromagnetic fields. While the E_z and the H_y dominate the electric and magnetic fields respectively in both of the backscattering and forward-scattering, the contribution from the E_x and the H_x field components is not significant. In the forward-scattering, the E_y and the H_z components also contribute considerably to the total fields, showing a large cross-polarized effect.

4. CONCLUSION

In this paper, the generalized multipole technique is successfully applied to characterize electromagnetic scattering from a gyrotropic bianisotropic cylinder of arbitrarily shaped cross section. The radar cross sections and near-zone fields of several scatterers have been computed. They are, namely, scattering of TE- and TM-polarized plane wave by (1) a chiral circular cylinder, (2) a chiral square cylinder, (3) a gyrotropic bianisotropic circular cylinder, and (4) a gyrotropic bianisotropic "lens" cylinder. Computed results obtained using the present generalized multipole technique for the chiral and gyrotropic bianisotropic cylinders are found to be in excellent agreement with exact solutions.

REFERENCES

1. Bohren, C. F., "Scattering of electromagnetic waves by an optically active cylinder," *J. Colloid Interface Sci.*, Vol. 66, 105–109, 1978.
2. Bohren, C. F., "Light scattering by an optically active sphere," *Chem. Phys. Lett.*, Vol. 29, 458–462, 1974.
3. Uslenghi, P. L. E., "Scattering by an impedance sphere coated with chiral layer," *Electromagn.*, Vol. 10, 201–211, 1990.
4. Kluskens, M. S. and E. H. Newman, "Scattering by a multilayer chiral cylinder," *IEEE Trans. Antennas Propagat.*, Vol. 39, 91–96, Jan. 1991.
5. Kluskens, M. S. and E. H. Newman, "Scattering by a chiral cylinder of arbitrary cross section," *IEEE Trans. Antennas Propagat.*, Vol. 38, 1448–1455, Sept. 1990.
6. Al-Kanhal, M. A. and E. Arvas, "Electromagnetic scattering from a chiral cylinder of arbitrary cross section," *IEEE Trans. Antennas Propagat.*, Vol. 44, 1041–1048, July 1996.
7. Zhang, M. and W. X. Zhang, "Scattering of electromagnetic waves from a chiral cylinder of arbitrary cross section — GMT approach," *Microwave & Opt. Technol. Lett.*, Vol. 10, No. 1, 22–25, 1995.
8. Monzon, J. C., "Scattering by a biisotropic body," *IEEE Trans. Antennas Propagat.*, Vol. 43, 1288–1296, Nov. 1995.
9. Olyslager, F., "Time-harmonic two- and three-dimensional closed-form Green's dyadics for gyrotropic, bianisotropic and anisotropic media," *Electromagn.*, Vol. 17, No. 4, 369–386, 1997.
10. Zhang, M. and W. Hong, "Electromagnetic scattering by a bianisotropic cylinder," *Proc. IEEE Antennas Propagat. Soc. Int. Symp.*, 910–913, Montreal Canada, July 1997.
11. Cheng, D. J., "Vector-wave-function theory of uniaxial bianisotropic semiconductor material," *Phys. Rev. E*, Vol. 56, No. 2, 2321–2324, 1997.
12. Yin, W. Y. and L. W. Li, "Multiple scattering from gyrotropic bianisotropic cylinders of arbitrary cross sections using the modeling technique," *Phys. Rev. E*, Vol. 60, No. 1, 918–925, 1999.
13. Shanker, B., S. K. Han, and E. Michielssen, "A fast multipole approach to analyze scattering from an inhomogeneous bianisotropic object embedded in a chiral host," *Radio Sci.*, Vol. 33, No. 1, 17–31, 1998.
14. Hafner, C., *The Generalized Multipole Technique for Computa-*

tional Electromagnetics, Artech House, Inc., 1991.

15. Leviatan, Y., P. G. Li, A. T. Adams, and J. Perini, "Single-post inductive obstacle in rectangular waveguide," *IEEE Trans. Microwave Theory Tech.*, Vol. 31, 806–811, Oct. 1983.
16. Leviatan, Y. and A. Boag, "Analysis of electromagnetic scattering from dielectric cylinders using a multifilament current model," *IEEE Trans. Antennas Propagat.*, Vol. 35, 1119–1127, Oct. 1987.
17. Leviatan, Y., Am. Boag, and Al. Boag, "Generalized formulations for electromagnetic scattering from perfectly conducting and homogeneous material bodies — theory and numerical solution," *IEEE Trans. Antennas Propagat.*, Vol. 36, 1722–1734, Dec. 1988.
18. Cheng, C. H., "GMT/SDT for underground EM scattering," Ph.D. dissertation, Southeast University, China, 1993 (In Chinese).
19. Na, H. G. and H. T. Kim, "Scattering analysis of conducting bodies of revolution using fictitious currents and point-matching," *IEEE Trans. Antennas Propagat.*, Vol. 43, 426–430, Apr. 1995.
20. Zhang, M. and Y. Shu, "Generalized multipole technique for electromagnetic scattering by arbitrarily shaped two-dimensional objects," *Microwave & Opt. Technol. Lett.*, Vol. 10, No. 6, 363–365, 1995.
21. Na, H. G. and H. T. Kim, "Convergence of the fictitious current model," *IEE. Proc. — H*, Vol. 143, No. 2, 163–168, 1996.
22. Kang, T. W. and H. T. Kim, "Basis function considerations for the methods of moments using the fictitious current model," *IEEE Trans. Antennas Propagat.*, Vol. 47, No. 6, 1118–1120, June 1999.
23. Beker, B., K. R. Umashankar, and A. Taflove, "Numerical analysis and validation of the combined field surface integral equations for electromagnetic scattering by arbitrary shaped two-dimensional anisotropic objects," *IEEE Trans. Antennas Propagat.*, Vol. 37, No. 12, 1573–1581, Dec. 1989.